Journal of Alloys and Compounds 509 (2011) 3441–3451

Contents lists available at ScienceDirect

Journal of Alloys and Compounds

journal homepage: www.elsevier.com/locate/jallcom

Spectroscopic and crystal-field analysis of energy levels of Eu^{3+} in SnO_2 in comparison with ZrO_2 and TiO_2

C.-G. Ma*, M.G. Brik, V. Kiisk, T. Kangur, I. Sildos

Institute of Physics, University of Tartu, Riia 142, Tartu, 51014, Estonia

ARTICLE INFO

Article history:
Received 25 November 2010
Received in revised form 3 December 2010
Accepted 9 December 2010
Available online 16 December 2010

Keywords:
Eu^{3+}:SnO_2
TiO_2
J-mixing
Crystal-field strength
Crystal-field splitting

ABSTRACT

We have carried out systematic crystal-field energy level calculations of Eu^{3+} ions doped in SnO_2 based on experimentally acquired luminescence spectra. In addition, with an aim of revealing systematic trends in spectra and crystal-field effects for Eu^{3+} ion in similar hosts, we have analyzed the TiO_2 (anatase):Eu^{3+} spectra as well. The obtained crystal-field parameters yield very good agreement between the calculated and observed energy levels. Emphasis has been put on analysis of the crystal-field-induced *J*-mixing effects and their roles in getting proper sets of crystal-field parameters and energy levels. A more general theory concerning *J*-mixing effects has been proposed and the relevant results will be valuable to understanding of the spectral characteristics of Eu^{3+} f–f transition spectra in other hosts. Relations between the maximum crystal-field splitting of some selected *J*-manifolds with $J=1$ and $J=2$ and crystal-field invariants have been re-visited and re-derived. The corresponding numbers of crystal-field parameters influencing the splitting of these manifolds have been taken into account in every case. The derived equations have been tested in applications to three systems (SnO_2, TiO_2 (three sites) and ZrO_2). Consistent results have been obtained, which confirms validity of the performed crystal-field analysis and opens a way for possible applications of the suggested calculating technique to other rare-earth ions.

1. Introduction

Wide-gap ($E_g > 3$ eV) semiconductors like SnO_2 (stannia), TiO_2 (titania) or ZrO_2 (zirconia) are technologically interesting since, due to an efficient energy transfer from host to rare-earth (RE) activators, these materials could be employed in the form of very thin phosphor layers and impose the potential of carrier-mediated excitation of RE ions yet providing transparency throughout the visible range and reduced thermal quenching of RE emission [1–3]. Moreover, such doped oxides are relatively easily prepared in various morphologies employing "soft" wet chemistry techniques.

For applications in lighting or displays, one is interested in the precise emission colour of incorporated activators. This can markedly depend on the crystal-field (CF) strength and local site symmetry as determined by the host matrix. In the case of RE^{3+} inclusions, the CF around the emission center can greatly influence the relative intensities as well as the amount of splitting of various 4f–4f transitions. Therefore, designing fruitful host–guest systems for precise tuning of luminescence properties presumes systematic understanding of the CF influence on RE energy levels.

Hereby, we conducted an in-depth CF analysis of energy level splitting of Eu^{3+} in SnO_2. A several-steps fitting procedure of the CF energy levels for multiplets with small *J* values has been proposed, where the values of the unit tensor operators U_k ($k=2$, 4, 6) between these interesting *J* manifolds have been re-calculated to improve the fitting calculation accuracy by taking into account non-diagonal elements of the free-ion's Hamiltonian between the terms with the same quantum numbers *S* and *L*. Besides, a particular attention has been paid to intricate effects of the CF states mixture, which manifest themselves in a different way for different CF states. It was shown that *J*-mixing effects can not only break down the "Judd-Ofelt" selection rules of 4f–4f transitions but also change the barycenter position and CF splitting of some *J* manifold, which, in turn, leads to the occurring of $^5D_0 \rightarrow {}^7F_0$ transition and a few wave numbers shift of the $^5D_0$ emitting state of Eu^{3+} ions.

The crystal-field parameters (CFPs) deduced for the SnO_2:Eu^{3+} system have been used as initial set of input parameters for calculations of the Eu^{3+} energy levels in two sites of another similar metal oxide: TiO_2.

Analysis of the Eu^{3+} energy level schemes in all considered hosts allowed to establish systematic trends in the maximum splitting of

* Corresponding author. On leave of absence from: College of Mathematics and Physics, Chongqing University of Posts and Telecommunications, Chongqing 400065, PR China. Tel.: +372 53064835; fax: +372 7383033.
E-mail address: chonggeng.ma@ut.ee (C.-G. Ma).

0925-8388/$ – see front matter © 2010 Elsevier B.V. All rights reserved.
doi:10.1016/j.jallcom.2010.12.071

some selected *J*-manifolds as functions of the CF strength. It was also shown that the CF-induced *J*-mixing is an important factor, which has to be considered for getting good agreement between the calculated and experimental energy level schemes of Eu^{3+} ions in crystals.

In the next sections we describe theoretical approach to the *J*-mixing problem, support this theoretical discussion by a number of examples, analyze them and after all we conclude the paper with a short summary.

2. Theoretical background and general analysis of Eu^{3+} energy levels in crystal field

2.1. CF Hamiltonian and energy levels

The standard form of the Hamiltonian acting within the $4f^N$ configuration of trivalent lanthanides in any host can be commonly written as [4]:

$$H = E_{avg} + \sum_{k=2,4,6} F^k f_k + \varsigma_f A_{so} + \alpha L(L+1) + \beta G(G_2) + \gamma G(R_7) + \sum_{i=2,3,4,6,7,8} T^i t_i + \sum_{h=0,2,4} M^h m_h + \sum_{k=2,4,6} P^k p_k + \sum_{k,q} B_q^k C_q^{(k)}, \quad (1)$$

where the notation and meanings of various operators and parameters are defined according to the standard practice [5,6]. In the above equation, all the terms except for the last one represent the "free-ion" Hamiltonian, whose parameters vary slightly from one host to another due to nephelauxetic effect [7], which is related to variation of the electron density distribution of rare-earth ions as influenced by the ligands. The last term describes the anisotropic components of the CF interactions; the B_q^k entries are referred to as the CFPs, and $C_q^{(k)}$ are the spherical operators. The number of non-zero CFPs B_q^k depends upon the site symmetry of the rare-earth ion position and increases with lowering the symmetry of the RE ion site.

In what follows we shall focus on description of the Eu^{3+} energy levels in three metal oxides MO_2 (M = Ti, Zr, Sn). It is well known that these oxides under ambient conditions have tetragonal or monoclinic crystal structures, in which the site-symmetry of the M^{4+} positions is one of these: D_{2d}, D_{2h}, C_{2h} and C_1 [8–11]. After doping, the RE ions occupy these M^{4+} positions; the site symmetry of these RE ion's sites can usually be assumed to be the same as before doping. Sometimes the actual symmetry can be somewhat lowered as a result of the lattice distortion caused by the ionic radii mismatch between the substituted and substituting ions and presence of the charge compensating oxygen vacancies near impurities. As an example, we mention here that in TiO_2:Eu^{3+} nanocrystals the site symmetry was changed from D_{2d} to D_2 or C_{2v} [12]. The generalized description of the M^{4+} site symmetries in the considered three MO_2 compounds allows for identification of four possible local symmetries of the M^{4+} sites: tetragonal, orthorhombic, monoclinic and triclinic [4]. However, it is always possible to simulate the CF energy levels of the Eu^{3+} $4f^6$ configuration only by employing the orthorhombic site symmetry (D_{2h}, D_2 and C_{2v}). For a higher symmetry site, this can be easily understood because the low-symmetry CFPs appearing after the local site symmetry is lowered can be directly set to zero. For the lower symmetry cases, this method can be explained by the fact that the orthorhombic C_{2v} symmetry group (often approximately replacing the monoclinic and triclinic symmetry groups) is an example of a point group with the highest symmetry, for which no CF degeneracy exists for non-Kramers' Eu^{3+} ions [13]. Thus, according to table 1.7 of Ref. [4], the CF Hamiltonian may be expressed in the following form:

$$H_{cf} = B_0^2 C_0^{(2)} + B_2^2 (C_2^{(2)} + C_{-2}^{(2)}) + B_0^4 C_0^{(4)} + B_2^4 (C_2^{(2)} + C_{-2}^{(2)}) + B_4^4 (C_4^{(4)} + C_{-4}^{(4)}) + B_0^6 C_0^{(6)} + B_2^6 (C_2^{(6)} + C_{-2}^{(6)}) + B_4^6 (C_4^{(6)} + C_{-4}^{(6)}) + B_6^6 (C_6^{(6)} + C_{-6}^{(6)}), \quad (2)$$

where all CFPs are real.

The theoretical CF energy levels can be obtained by diagonalizing the parameterized Hamiltonian matrix in the entire $\eta SLJM$ basis of the $4f^6$ electronic configuration of Eu^{3+} (*S, L, J, M* stand for the quantum numbers of the spin, orbital momentum, total momentum and its projection, respectively; η denotes all other quantum numbers needed to distinguish between the states with identical *S, L, J, M* sets). By minimizing the root-mean-square (rms) deviation between the theoretical and experimental CF energy levels, an optimized set of CFPs can be obtained and the complete energy level scheme (which is to be compared with experimental data) can be generated.

However, the fitting calculations cannot always be carried out, especially when only a few CF energy levels are observed and the number of fitting parameters is large enough in comparison to the number of the observed levels. For example, in the CF Hamiltonian described by Eq. (2), at least 9 CFPs plus one energy barycenter can be varied.

When the CF effects in powdered samples are studied, it is generally difficult to acquire adequate absorption spectra due to the complicated sample morphology. In this case one must rely on luminescence spectra, but they can give information only about a few energy levels. In addition, a particular difficulty is related to fitting of the CF energy levels with a large *J* quantum number ($J \geq 3$), which are not very clearly observed and distinguished in the experimental spectra. In this case, determination of the sixth-rank CFPs will be difficult and even impossible due to the selection rule ($k \leq 2J$, k is the CFPs rank) for the CF matrix elements among the $J \geq 3$ multiplet. It is also worthwhile to note that in some centro-symmetric systems, the spectra of rare-earth ions are essentially vibronic in character; several vibronic transition bands coming from one single CF energy level will hide the neighboring levels. As a result, a lot of ambiguity will be brought into analysis of the zero-phonon lines' positions in these systems [14]. All these factors can cause uncertain assignment of the CF energy levels; moreover, an unrealistic CFPs set can be obtained. To overcome this problem, a several-steps fitting procedure can be suggested, based on ignoring the *J*-mixing effect. Subsequent diagonalization of the CF matrices for the multiplets with small *J* values (J = 1 or 2) can be used to obtain estimates of the second and fourth rank CFPs from the experimental emission spectra. According to this idea, an effective Hamiltonian of $4f^6$ configuration for Eu^{3+} ions within one $[\eta^{2S+1}L]_J$ multiplet can be expressed as follows:

$$H([\eta^{2S+1}L]_J) = E([\eta^{2S+1}L]_J) + H_{cf} = E_{cf}([\eta^{2S+1}L]_J) + H_{cf}, \quad (3)$$

where H_{cf} represents the CF operator (which is determined in the sub-space spanned by the wave functions of this *J*-manifold only; it can have only the second rank (for J = 1) or the second and fourth ranks (for J = 2) contributions) and "[]" represents the $\eta^{2S+1}L$ as the dominant component of this *J* multiplet, where the ηSL states are actually mixed due to "free-ion" interactions (the Coulomb interaction, most of all). Here $E([\eta^{2S+1}L]_J)$ is the barycenter of the experimental CF energy levels of this multiplet (i.e. $E_{cf}([\eta^{2S+1}L]_J)$, which in the first approximation is equal to the free-ion energy level of the $[\eta^{2S+1}L]_J$ multiplet. This scheme is suitable for modeling the CF splitting of the $[^7F]_J$ and $[^5D]_J$ multiplets (J = 1 and 2) of Eu^{3+} ions. These manifolds are easily observed in the emission and absorption spectra of Eu^{3+} ions doped in MO_2.

Table 1
The non-zero and upper triangle H_{cf} matrix elements within $[\eta^{2S+1}L]_2$ multiplet of Eu^{3+} ions doped in MO_2. (unit: cm^{-1}).

$H_{00} = \frac{2\sqrt{2}}{5\sqrt{3}}\overline{U^2([\eta^{2S+1}L]_2)}B_0^2 + \frac{-2}{\sqrt{55}}\overline{U^4([\eta^{2S+1}L]_2)}B_0^4$	$H_{02} = H_{-20} = \frac{-2\sqrt{2}}{5\sqrt{3}}\overline{U^2([\eta^{2S+1}L]_2)}B_2^2 + \frac{1}{\sqrt{33}}\overline{U^4([\eta^{2S+1}L]_2)}B_2^4$
$H_{11} = H_{-1-1} = \frac{\sqrt{2}}{5\sqrt{3}}\overline{U^2([\eta^{2S+1}L]_2)}B_0^2 - \frac{4}{3\sqrt{55}}\overline{U^4([\eta^{2S+1}L]_2)}B_0^4$	$H_{-22} = \frac{\sqrt{14}}{3\sqrt{11}}\overline{U^4([\eta^{2S+1}L]_2)}B_4^4$
$H_{22} = H_{-2-2} = \frac{-2\sqrt{2}}{5\sqrt{3}}\overline{U^2([\eta^{2S+1}L]_2)}B_0^2 + \frac{1}{3\sqrt{55}}\overline{U^4([\eta^{2S+1}L]_2)}B_0^4$	$H_{-11} = \frac{-2}{5}\overline{U^2([\eta^{2S+1}L]_2)}B_2^2 - \frac{2\sqrt{2}}{3\sqrt{11}}\overline{U^4([\eta^{2S+1}L]_2)}B_2^4$

Notes: $H_{MM'}$ represents the crystal-field matrix elements $\langle[\eta^{2S+1}L]_{2M}|H_{cf}|[\eta^{2S+1}L]_{2M'}\rangle (M = -2\ldots2, M' = M+1\ldots2)$. $\overline{U^2([\eta^{2S+1}L]_2)}$ and $\overline{U^4([\eta^{2S+1}L]_2)}$ are respectively the RMEs of the unitary tensor $U^{(2)}$ and $U^{(4)}$ between $[\eta^{2S+1}L]_2$ multiplets, and can be referred to in Table 2.

For the simplest case of $J = 1$ multiplets, the splitting can be well described only by the second-rank CFPs due to the selection rule of CF matrix elements (matrix elements of the fourth and sixth rank operators in the CF Hamiltonian are identically zero if $J = 1$). In the orthorhombic site symmetry, the $2J + 1 = 3$ fold degeneracy of the $^{2S+1}L_1$ multiplet of Eu^{3+} ions will be removed completely, and three energy levels arising from the $J = 1$ multiplets will be detected. After diagonalization of the $H([\eta^{2S+1}L]_1)$ matrix using the JM basis set ($J = 1$ and $M = 0, \pm 1$), the energies of three CF components are as follows:

$$\begin{aligned}
E_{|0\rangle} &= E_{cf}([\eta^{2S+1}L]_1) + \frac{2\sqrt{14}}{15}\overline{U^2([\eta^{2S+1}L]_1)}B_0^2 \\
E_{|-1,1\rangle^-} &= E_{cf}([\eta^{2S+1}L]_1) - \frac{\sqrt{14}}{15}\overline{U^2([\eta^{2S+1}L]_1)}B_0^2 \\
&\quad + \frac{2\sqrt{7}}{5\sqrt{3}}\overline{U^2([\eta^{2S+1}L]_1)}B_2^2 \\
E_{|-1,1\rangle^+} &= E_{cf}([\eta^{2S+1}L]_1) - \frac{\sqrt{14}}{15}\overline{U^2([\eta^{2S+1}L]_1)}B_0^2 \\
&\quad - \frac{2\sqrt{7}}{5\sqrt{3}}\overline{U^2([\eta^{2S+1}L]_1)}B_2^2
\end{aligned} \quad , \tag{4}$$

where $|-1,1\rangle^- = i/\sqrt{2}\left(|-1\rangle + |+1\rangle\right)$, $|-1,1\rangle^+ = 1/\sqrt{2}\left(|-1\rangle - |+1\rangle\right)$, and $|-1\rangle$, $|+1\rangle$ denote two wave functions of the $J = 1$ state with quantum numbers $M = -1$ and $M = 1$, respectively; $\overline{U^2([\eta^{2S+1}L]_1)}$ represents the reduced matrix element (RME) of the unit tensor operator $U^{(2)}$ between the $[\eta^{2S+1}L]_1$ free-ion's multiplets. In the above derivation, the matrix elements of CF interactions can be obtained by referring to the formulae (1.20) and (1.37) of Ref. [4] and the involved 3*j* and 6*j* symbol values can be found in Ref. [15]. We point out here that the CF eigenvalues of the $J = 1$ multiplet given in Eqs. (179) and (180) of Ref. [13] reveal one misprint, which has been corrected in Eq. (4) above. It should be kept in mind, however, that there exists ambiguity in the assignment of three observed energy levels to those theoretical three, which may result in six sets of different CFPs under the different permutations of the assignments. This is because three orthogonal and equivalent crystallographic axes will offer six kinds of equivalent choices of the *xyz* coordinate systems in the orthorhombic symmetry groups, although the CF Hamiltonian still preserves the form of Eq. (2) in each of these coordinate systems. The six sets of CFPs with different magnitude or sign generate fully identical CF splitting patterns. The conversion relation between any two sets of CFPs can be easily obtained from Ref. [16], and a misprint in the last reference needs to be corrected as pointed out by Rudowicz et al. [17].

For the $J = 2$ multiplets, the orthorhombic CF also completely removes the five-fold degeneracy. The second (obtained after diagonalization of the $J = 1$ matrix) and the fourth rank CFPs should be used simultaneously to describe the CF splitting for these states, which is not influenced by the sixth order CFPs. The non-zero and upper triangle H_{cf} matrix elements within the $[\eta^{2S+1}L]_2$ multiplet are shown in Table 1. However, the analytical expressions for the CF energy levels cannot be directly provided because of a large number of non-diagonal matrix elements.

As seen from Eq. (4) and Table 1, the RMEs of the unitary tensor operators $U^{(k)}$ between the $[\eta^{2S+1}L]_J$ multiplets (or $\overline{U^k([\eta^{2S+1}L]_J)}$ for short, hereafter) can be considered as parameters. When the CFPs are fixed, the calculated CF splitting will be directly determined by these RME values. Thus, it is necessary to pay more attention to their values. $\overline{U^k([\eta^{2S+1}L]_J)}$ is not the single $U^{(k)}$ RME between the dominative $\eta^{2S+1}L_J$ components, but includes the contributions of all $\eta^{2S+1}L_J$ components with different ηSL and identical J quantum numbers. With the help of the formula (1.38) of Ref. [4], $\overline{U^k([\eta^{2S+1}L]_J)}$ can be expressed as follows:

$$\begin{aligned}
\overline{U^k([\eta^{2S+1}L]_J)} = \sum_{\eta'S'L'\eta''S''L''} & C_{\eta'S'L'}C_{\eta''S''L''}(-1)^{S'+L''+J+k}\delta_{s's''}\cdot(2J+1) \\
& \cdot \begin{Bmatrix} J & J & k \\ L'' & L' & S' \end{Bmatrix} \left\langle \eta'S'L' \left\| U^{(k)} \right\| \eta''S''L'' \right\rangle ,
\end{aligned} \tag{5}$$

where $C_{\eta'S'L'}$ are the mixing coefficients of the state $|4f^6\eta'S'L'J\rangle$ occurring in the intermediate coupling basis $[\eta^{2S+1}L]_J$, the curly bracket $\{\ldots\}$ is a 6*j* symbol [15] and the last term is the single RME between the *LS* spectral terms that has been tabulated by Nielson and Koster [18]. This means these RMEs rely on the knowledge of the composition of free-ion wave functions, which are relatively insensitive to hosts. Therefore, their values can usually be regarded in a good approximation as constants. Although their squares were given by Carnall et al. [19], they still need to be re-calculated because the signs of these RMEs are critical to CF calculations. The $\overline{U^k([\eta^{2S+1}L]_J)}$ values for $[^7F]_J$ and $[^5D_{(3)}]_J$ ($J = 1-3$) are evaluated and collected in Table 2 by applying the Eq. (5) and the free-ion wave functions generated by one free-ion calculation using the free-ion parameter values from Ref. [5]. As a comparison, the $U^{(k)}$ RMEs without taking ηSL mixing into account are also evaluated and listed in Table 2. It is easy to see from Table 2, that the ηSL mixing produces a small difference between the RME for the $[^7F]_J$ states, but has a profound influence on the RME for the $[^5D_{(3)}]_J$ manifolds, affecting not only the absolute value, but also the sign as well (which, eventually, affects the order of the CF energy levels).

By combining Eq. (4) and Tables 1 and 2, one can easily give estimates of the second and fourth rank CFPs from the experimental emission spectra. However, the *J*-mixing effect caused by the CF interaction (which can mix up states with different *J*, *M* values) has a certain influence on the CF splitting of the $J = 1$ and $J = 2$ multiplets, and cannot be simply ignored. Actually, the *J*-mixing effect depends strongly on the energy intervals between the *J* manifolds involved and in some (but not all) cases can be omitted without any lack of accuracy. For example, for the $[^5D_{(3)}]$ term of free Eu^{3+} ions (located at about 17,000 cm^{-1}), the energy separations between the $[^5D_{(3)}]_J$ states ($J = 0, 1, 2$) are much larger (about or above 2000 cm^{-1}) and the RME of the $U^{(k)}$ operators between the $[^5D_{(3)}]_J$ manifolds are also much smaller than the corresponding values for the $[^7F]_J$ manifolds as shown in Table 2. So in this case consideration of the *J*-mixing is not necessary for the $[^5D_{(3)}]_J$ multiplet, but is highly advisable for the closely located $[^7F]_J$ multiplets. In the following, *J*-mixing will be given detailed consideration within ^7F term with an aim of revealing their effects upon the CF splitting for minimizing the deviation between the experimentally deduced and theoretically calculated energy levels.

Table 2
The $\overline{U^k([\eta^{2S+1}L]_J)}$ RME (J = 1–3) within [^{7}F] and [^{5}D$_{(3)}$] terms with and without taking into account the ηSL mixing (free-ion Hamiltonian parameters were taken from Ref. [5]).

Multiplets	k = 2		k = 4		k = 6	
	Isolated term	ηSL mixing	Isolated term	ηSL mixing	Isolated term	ηSL mixing
[^{7}F]$_1$	0.4009	0.3925	–	–	–	–
[^{7}F]$_2$	0.3208	0.3163	−0.3532	−0.3493	–	–
[^{7}F]$_3$	0.1667	0.1662	0.1667	0.1612	0.1667	0.1677
[^{5}D$_{(3)}$]$_1$	−0.1260	0.1149	–	–	–	–
[^{5}D$_{(3)}$]$_2$	−0.0589	0.03341	0.0898	0.0844	–	–
[^{5}D$_{(3)}$]$_3$	0.0673	−0.1256	−0.2332	−0.0482	0	0.0580

2.2. Wave functions and J-mixing

J-mixing effect caused by the non-diagonal matrix elements of CF interaction between different J multiplets can influence the composition of wave functions and thus intensity of the transitions between different states. In this way initially completely forbidden $^5D_0 \rightarrow {}^7F_0$ transition becomes partially allowed due to "borrowing" some intensity from the $^5D_0 \rightarrow {}^7F_J$ (J = 2, 4 and 6) transitions. To show and understand this mixing effect on the components of wavefunctions, we firstly use the perturbation method to define the average mixing percentage from one $^7F_{J'}$ multiplet into any CF state of another ^7F_J multiplet as follows:

$$\alpha(J' \rightarrow J) = \frac{1}{2J+1} \sum_{\substack{M=-J\cdots J \\ M'=-J'\cdots J'}} \left| \frac{\left\langle {}^7F_{J'M'} \left| H_{cf} \right| {}^7F_J \right\rangle}{E({}^7F_J) - E({}^7F_{J'})} \right|^2$$

$$= \sum_{k=2,4,6} \frac{N_v^2(B^k)}{4\pi \times (2J+1)} \left| \frac{\left\langle {}^7F_J \left\| U^{(k)} \right\| {}^7F_{J'} \right\rangle \left\langle f \left\| c^{(k)} \right\| f \right\rangle}{E({}^7F_J) - E({}^7F_{J'})} \right|^2, \quad (6)$$

where the derivation is similar to Eq. (10) of Ref. [20], and $N_v(B^k)$ is the CF strength parameter including only the k-th rank CFPs written as follows:

$$N_v(B^k) = \sqrt{\sum_{q=-k}^{k} \frac{4\pi}{2k+1} \left| B_q^k \right|^2}, \quad (7)$$

as defined in Ref. [20]. Here $E(^7F_J)$ stands for the free-ion energy of the ^7F_J multiplet and can be approximately generated as 0, 383, 1054, 1918, 2906, 3969 and 5074 cm^{-1} for J = 0-6 by one free-ion calculation using the free-ion parameter values of Ref. [5]. $\langle {}^7F_J || U^{(k)} || {}^7F_{J'} \rangle$ and $\langle f || c^{(k)} || f \rangle$ are the RME of the multi-electron unit tensor $U^{(k)}$ and the single-electron spherical harmonic tensor $c^{(k)}$, respectively. For values of J from 0 to 3, by using Eq. (6), formulae (1.20) and (1.38) of Ref. [4] and tabulated RME for $U^{(k)}$ (k = 2,4,6) in Ref. [18], the composition of the $^7F_{0,1,2,3}$ levels has been expressed in terms of three CF strength parameters (Table 3). These wave functions obtained with taking into account the J-mixing effects can be readily used for the intensity calculation of the $^5D_0 \rightarrow {}^7F_0$ and $^5D_0 \rightarrow {}^7F_3$ transitions, as shown in Ref. [21]. It is instructive to estimate numerically, how strong such a mixture can be. If the order of magnitude of $N_v(B^k)^2$ is approximately taken as 10^6 cm^{-2} (which is a reasonable assumption based on numerous literature data), the mixing percentage in Table 3 can be approximately estimated. For the $^7F_0$ state, the admixture from the $^7F_2$ manifold (about 1.9%) is dominant and usually only considered in the intensity calculation of the $^5D_0 \rightarrow {}^7F_0$ transition, but when the square of the fourth rank CF strength parameter is one order greater than that of the second rank (i.e. 10^6 cm^{-2} for $N_v(B^2)^2$ and 10^7 cm^{-2} for $N_v(B^4)^2$), the contribution from the $^7F_4$ state (about 1.7%) has to be taken into account; the admixture of the $^7F_6$ states is completely ignored due to very small amount (not more than 0.8% even if the magnitude of $N_v(B^6)^2$ is 10^7 cm^{-2}). For the $^7F_1$ state, the contributions of the $^7F_{J'}$ multiplets with $J' > 3$ can be directly neglected, as not exceeding 0.8%. This also implies that the sixth rank CFPs can be safely dropped when calculating the CF splitting of the $^7F_1$ state. Meanwhile, it can be noticed that the contributions of the fourth rank CFPs will dominate for admixture from $^7F_3$ into $^7F_1$ if the magnitudes of $N_v(B^2)^2$ and $N_v(B^4)^2$ are respectively 10^6 cm^{-2} and 10^7 cm^{-2} (numerical estimations yield the values of about 1.9% for fourth rank and 0.45% for second rank; the total mixing percentage from $^7F_3$ is 2.33%). For the $^7F_2$ state, the contribution from the $^7F_3$ state is very important and larger (about 1.35%), and that from other high-lying ^7F_J state is not more than 0.6%. In addition, the sixth rank CFPs will have some influences on CF levels of $^7F_2$, especially the highest lying CF level, because there is the same weight respectively for fourth and sixth rank CF contributions in the admixture from $^7F_4$, $^7F_5$ and $^7F_6$. Thus, only considering the second and fourth rank CFPs for $^7F_2$ state will be a rough approximation.

2.3. J-mixing and barycenters of J-manifolds

Except for the influence on the wavefunctions, the maximum CF splitting of every ^7F_J multiplet is also changed, and the barycenters of the CF levels within ^7F_J multiplets are somewhat shifted relative to the free-ion levels generated by one "free-ion" calculation without any CFPs. As mentioned before, not all energy levels from the

Table 3
The average mixing percentage from one $^7F_{J'}$ multiplet into any crystal-field state of another ^7F_J multiplet (unit: $\times 10^{-6}$).

$\alpha(J' \rightarrow J)$	$^7F_0$	$^7F_1$	$^7F_2$	$^7F_3$	$^7F_4$	$^7F_5$	$^7F_6$
$^7F_0$	–	0	$1.91N_v^2(B^2)$%	0	$0.171N_v^2(B^4)$%	0	$0.072N_v^2(B^6)$%
$^7F_1$	0	–	$0.589N_v^2(B^2)$%	$0.45N_v^2(B^2)$% $+0.188N_v^2(B^4)$%	$0.0947N_v^2(B^4)$%	$0.0313N_v^2(B^4)$%	$0.0738N_v^2(B^6)$%
$^7F_2$	$0.382N_v^2(B^2)$%	$0.354N_v^2(B^2)$%	–	$0.758N_v^2(B^2)$% $+0.592N_v^2(B^4)$%	$0.194N_v^2(B^2)$% $+0.0041N_v^2(B^4)$% $+0.0246N_v^2(B^6)$%	$0.0757N_v^2(B^4)$% $+0.0637N_v^2(B^6)$%	$0.0059N_v^2(B^4)$% $+0.0761N_v^2(B^6)$%
$^7F_3$	0	$0.193N_v^2(B^2)$% $+0.0804N_v^2(B^4)$%	$0.542N_v^2(B^2)$% $+0.423N_v^2(B^4)$%	–	$0.854N_v^2(B^2)$% $+0.201N_v^2(B^4)$% $+0.302N_v^2(B^6)$%	$0.0881N_v^2(B^2)$% $+0.0887N_v^2(B^4)$% $+0.172N_v^2(B^6)$%	$0.0334N_v^2(B^4)$% $+0.079N_v^2(B^6)$%

Notes: The multiplets in the first column represent the dominative ^7F_J multiplets. Meanwhile, the mixing $^7F_{J'}$ multiplets are shown in the first row. The intersection of a row and a column is the average mixing percentage from one $^7F_{J'}$ multiplet into any crystal-field state of another ^7F_J multiplet.

^{7}F term are observed, which makes consideration of the J-mixing effect by the energy matrix diagonalization more difficult. The perturbation theory usually provides an approach to understand and take this effect into account without paying any attention to the CF splitting of the multiplets imposing perturbations, especially those of multiplets with $J \geq 3$ still relying on the unknown sixth rank CFP except for the second and fourth rank. Thus, by choosing the ^{7}F term with all possible J from 0 to 6 as the complete space and the studied ^7F_J (J = 0, 1 or 2) multiplets as a model-space, the effective Hamiltonian can be written in the following form [22]:

$$H_{eff} = E(^7F_J) + H_{cf} + \sum_{\substack{J'=0\cdots6,\ \neq J \\ M'=-J'\cdots J'}} \frac{H_{cf}\left|^7F_{J'M'}\right\rangle\left\langle^7F_{J'M'}\right|H_{cf}}{E(^7F_J) - E(^7F_{J'})}, \quad (8)$$

where the first term $E(^7F_J)$ is also the free-ion energy of the ^7F_J multiplet. The barycenter of all energy levels arising from one J manifold can also be obtained; it equals to the trace of the effective Hamiltonian matrix divided by $2J+1$ because of the trace invariance before and after diagonalization. Thus, an accurate analytical formula of the barycenters of the CF levels within ^7F_J multiplet can be written as:

$$E_{cf}(^7F_J) = \frac{1}{2J+1}\sum_{M=-J}^{J}\left\langle^7F_J\left|H_{eff}\right|^7F_J\right\rangle = E(^7F_J) + \sum_{k=2,4,6}\frac{N_v^2(B^k)}{4\pi\times(2J+1)}\sum_{J'=0\cdots6,\ \neq J} \times \frac{\left|\left\langle^7F_J\left\|U^{(k)}\right\|^7F_{J'}\right\rangle\left\langle f\left\|c^{(k)}\right\|f\right\rangle\right|^2}{E(^7F_J) - E(^7F_{J'})}. \quad (9)$$

The barycenters $E_{cf}(^7F_J)$ of the CF levels can usually be obtained from the measurements, so by following the same procedure of obtaining Table 3, we can express the corrected barycenters of the split free-ion energy levels for J = 0–2 as follows:

$$\begin{aligned} E(^7F_0) &= E_{cf}(^7F_0) + 2.01\times10^{-5}\times N_v^2(B^2) + 4.98\times10^{-6}\times N_v^2(B^4) \\ &\quad +3.66\times10^{-6}\times N_v^2(B^6) \\ E(^7F_1) &= E_{cf}(^7F_1) + 1.09\times10^{-5}\times N_v^2(B^2) + 6.39\times10^{-6}\times N_v^2(B^4) \\ &\quad +4.11\times10^{-6}\times N_v^2(B^6) \\ E(^7F_2) &= E_{cf}(^7F_2) + 3.75\times10^{-6}\times N_v^2(B^2) + 7.64\times10^{-6}\times N_v^2(B^4) \\ &\quad +5.37\times10^{-6}\times N_v^2(B^6) \end{aligned} \quad (10)$$

From the above equation, it can be deduced that the J-mixing effect results in pushing the free-ion energy levels $E(^7F_J)$ upward because of interaction with other high-lying ^7F_J multiplets. The contributions of the sixth rank CF strength parameter are not greater than 5 cm^{-1} for the free-ion level of $^7F_1$ relative to $^7F_0$, if the square of the sixth rank CF strength parameter is estimated as 10^7 cm^{-2}. Taking Eqs. (8) and (10) simultaneously, we obtain the final expression of the effective Hamiltonian taking J-mixing effect into account:

$$H_{eff} = E_{cf}(^7F_J) + H_{cf} + \sum_{\substack{J'=0\cdots6,\ \neq J \\ M'=-J'\cdots J'}} \frac{H_{cf}\left|^7F_{J'M'}\right\rangle\left\langle^7F_{J'M'}\right|H_{cf}}{E(^7F_J) - E(^7F_{J'})} - \sum_{k=2,4,6}\frac{N_v^2(B^k)}{4\pi\times(2J+1)}\sum_{J'=0\cdots6,\ \neq J}\frac{\left|\left\langle^7F_J\left\|U^{(k)}\right\|^7F_{J'}\right\rangle\left\langle f\left\|c^{(k)}\right\|f\right\rangle\right|^2}{E(^7F_J) - E(^7F_{J'})} \quad (11)$$

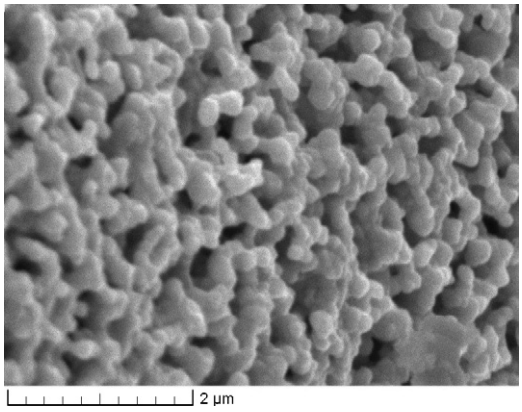

Fig. 1. SEM image of sol–gel-prepared SnO_2:Eu powder annealed at 1400 °C.

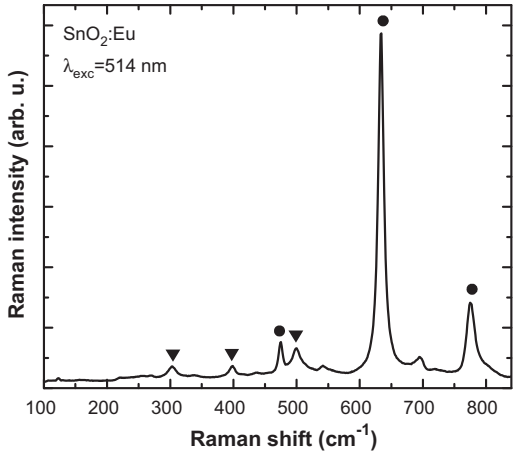

Fig. 2. Raman spectrum of sol–gel-prepared SnO_2:Eu powder annealed at 1400 °C. The circles mark the peaks due to SnO_2 while the peaks indicated by triangles were assigned to $Eu_2Sn_2O_7$ [24].

If in Eq. (11) the denominators of the last two terms are approximately replaced by differences between the free-ion energy levels, the procedure of fitting the calculated CF energy levels to the experimental ones will be reduced to varying the CFPs only.

3. Applications to the crystal-field analyses of Eu^{3+} ions doped in MO_2

3.1. SnO_2:Eu^{3+}

0.5 at% europium-doped SnO_2 was prepared using a sol–gel route based on $Sn(OPr)_4$ and $EuCl_3{}^*xH_2O$ as precursors (see [23] for details). The as-prepared dried and grinded powder was annealed at 1400 °C in air leading to a fine nanoparticulate powder with characteristic particle size of ~250 nm as seen by SEM (Fig. 1). The crystal structure and phase content was detected by Raman spectroscopy using the Renishaw inVia microspectrometer. The Raman spectrum (Fig. 2) indicates strong peaks due to the cassiterite phase of SnO_2. Still, traces of pyrochlore $Eu_2Sn_2O_7$ also seem to be present which is apparently the result of a limited solubility of Eu in SnO_2 matrix [24]. The annealed sample produces fairly bright emission due to Eu^{3+}. For acquisition of luminescence spectra, a tunable optical parametric oscillator (emitting nanosecond pulses) was employed for excitation whereas a CCD-equipped spectrometer was used for detection (spectral resolution <2 nm). The luminescence spectrum excited at 464 nm (corresponding to the

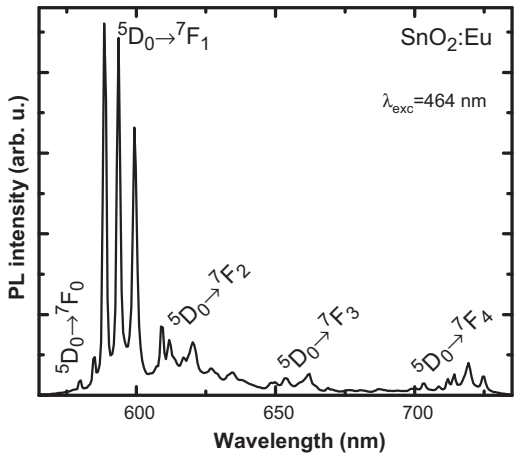

Fig. 3. Photoluminescence spectrum of sol–gel-prepared SnO_2:Eu powder excited at 464 nm and measured at room temperature. The spectrum is corrected to instrumental response.

$^7F_0 \rightarrow {}^5D_2$ absorption transition of Eu^{3+}) and measured at room temperature is shown in Fig. 3. Clearly resolved fine structure of the various $^5D_0 \rightarrow {}^7F_J$ (J = 0–4) transitions of Eu^{3+} is observed indicating that Eu^{3+} ions are incorporated into crystalline surrounding. Practically identical spectrum was obtained under host-sensitized excitation at 266 nm which suggests that the emission from one main type of Eu^{3+} centers is prevailing. In spite of the possible traces of $Eu_2Sn_2O_7$ present, the luminescence spectrum is very similar to those reported previously by Blasse et al. [25] and Grabtree [9] on Eu^{3+} in SnO_2.

As can be seen from Fig. 3, intensity of the magnetic dipole transition ($^5D_0 \rightarrow {}^7F_1$) at about 580 – 600 nm is much stronger than that of the induced electric dipole transitions ($^5D_0 \rightarrow {}^7F_2$) at about 620 nm. This indicates the local environment around the Eu^{3+} ions to be centro-symmetric, as the site symmetry of the Sn^{4+} ions substituted by Eu^{3+} ions is D_{2h} or C_{2h}. Thus, the assignment of CF energy levels of ^7F_J multiplets with larger J values, such as J = 3 or 4, is very difficult to be carried out because of the vibronic transitions' influence, as mentioned in Section 2. Although the CF fitting calculations using the full matrix diagonalization within ^7F_J (J = 0. . .6) term will be not implemented due to the lack of the $^7F_3$ CF energy levels, this spectrum will be a good example for testing our theory in Section 2. The observed CF energy levels of other ^7F_J multiplets (J = 0–2) are listed in Table 4.

At first, we ignored the J-mixing effect to respectively deal with the CF energy levels of the $^7F_1$ and $^7F_2$ manifolds, which means only the first-order correction caused by CF Hamiltonian is considered from the viewpoint of perturbation theory as the last term is given up in Eq. (8). Following this approximation, we could directly use

Table 5
Optimized parameters for Eu^{3+} ions doped in SnO_2 (unit: cm^{-1}).

Parameter	No J-mixing	J-mixing
F^2	82601	82061
ξ_{4f}	1327	1317
N_E (free)	4	4
N_p (free)	2	2
σ (free)	29	25
B^2_0	777	936
B^2_2	298	501
B^4_0	−1697	−1814
B^4_2	−1172	−1046
B^4_4	−575	−832
N_E(cf)	9	9
N_p(cf)	5	5
σ(cf)	8	44

Notes: The ratios of F^4 and F^6 to F^2 and other free-ion parameter values were fixed at the values given in Ref. [5]. N_E and N_p are the numbers of experimental levels fitted and the numbers of symbols "cf" and "free" in brackets, respectively, represent the crystal-field and free-ion calculations. $\sigma(\text{free}) = \sqrt{\sum_{i=1,\cdots N_E(\text{free})}(E_i(\text{calc.}) - E_i(\text{exp.}))^2/(N_E(\text{free}) - N_p(\text{free}))}$; $\sigma(cf) = \sqrt{\sum_{i=1,\cdots N_E(cf)}(E_i(\text{calc.}) - E_i(\text{exp.}))^2/(N_E(cf) - N_p(cf))}$.

Eq. (4), the experimental value of $E_{cf}(^7F_1)$ and the standard value of the $\overline{U^2(^7F_1)}$ matrix element to obtain two CFPs with k = 2. The choice of the initial axis system for the CF analysis is arbitrary and there are six sets of different CFPs, as discussed in Section 2. One set of CFPs is usually reported, under which the $E_{|0>}$ level is assigned as the highest $^7F_1$ stark level while the $E_{|-1,1>^-}$ and $E_{|-1,1>^+}$ states correspond to the middle and lowest $^7F_1$ Stark levels, respectively. To further obtain three CFPs values with k = 4, we finished a fitting calculation within the $^7F_2$ multiplet by diagonalizing the parameterized CF matrix provided by Table 1. In this calculation, the values of two second rank CFPs were fixed (as obtained from the CF analysis of the $^7F_1$ state); the experimental values of $E_{cf}(^7F_2)$ and the standard values of $\overline{U^2(^7F_2)}$ and $\overline{U^4(^7F_2)}$ were used. The obtained second and fourth rank CFPs are listed in Table 5, whereas Table 4 shows the calculated energy levels in comparison with the experimental data. The free-ion energy levels for ^7F_J (J = 0–2) and $^5D_0$ listed in Table 6 are respectively equal to the gravity centers of their CF levels in this approximation without considering J-mixing, so a fitting calculation of free-ion levels was made by utilizing the f-shell programs of M.F. Reid, where only F^2 and ξ_{4f} parameters were allowed to vary freely while the ratios of F^4 and F^6 to F^2 and other free-ion parameter values were fixed at the values given in Ref. [5]. The finally obtained F^2 and ξ_{4f} parameters are collected in Table 5 whereas Table 6 shows the calculated free-ion energy levels.

Secondly, we began to take J-mixing effect into account to discuss the CF splitting of $^7F_1$ and $^7F_2$. To have a first impression of understanding J-mixing, we evaluated the mixing percentages from

Table 4
Observed (E_{exp}) and calculated (E_{calc}) CF energy levels of Eu^{3+} ions doped in SnO_2 (unit: cm^{-1}).

Multiplets	No J-mixing			J-mixing		
	E_{calc}	E_{exp}	$\Delta = E_{exp} - E_{calc}$	E_{calc}	E_{exp}	$\Delta = E_{exp} - E_{calc}$
$^7F_0$	0	0	0	0	0	0
$^7F_1$	266	266	0	276	266	−10
	412	412	0	428	412	−16
	572	572	0	547	572	25
$^7F_2$	826	836	10	842	836	−6
	918	912	−6	896	912	16
	1057	1048	−9	1019	1048	29
	1138	1137	−1	1108	1137	29
	1306	1312	6	1380	1312	−68

Notes: The standard deviations for two cases are respectively 8 cm^{-1} and 44 cm^{-1}. The sixth rank CFPs are ignored in the J-mixing calculation as not contributing to the splitting of the multiplets shown in the table.

Table 6
Observed (or presumed) and calculated free-ion energy levels of Eu^{3+} ions doped in SnO_2 (unit: cm^{-1}).

Multiplets	No J-mixing			J-mixing			The average mixing components in any crystal-field state of free-ion level
	E_{calc}	E_{exp}	$\Delta = E_{exp} - E_{calc}$	E_{calc}	E_{free}	$\Delta = E_{free} - E_{calc}$	
$^7F_0$	14	0	−14	−10	0	10	$95.01\%^7F_0 + 3.56\%^7F_2 + 1.43\%^7F_4$
$^7F_1$	393	417	24	366	389	23	$95.42\%^7F_1 + 1.11\%^7F_2 + 2.41\%^7F_3 + 0.80\%^7F_4 + 0.26\%^7F_5$
$^7F_2$	1058	1049	−9	1026	1001	−25	$0.69\%^7F_0 + 0.64\%^7F_1 + 91.52\%^7F_2 + 6.12\%^7F_3 + 0.38\%^7F_4 + 0.60\%^7F_5 + 0.05\%^7F_6$
$^5D_0$	17259	17259	0	17129	17121	−8	–

Notes: E_{calc} represents the fitting calculation values of free-ion energy levels. E_{free} means the presumed free-ion's energy levels (i.e. the corrected barycenters of split free-ion energy levels) form the Eq. (10) when J-mixing taking into account, whereas E_{exp} stands for the measured barycenters of the CF energy levels and can be treated as the free-ion energy levels when J-mixing not considered. The standard deviations for two cases are, respectively, 29 cm^{-1} and 25 cm^{-1}. The J-mixing effect is ignored for $^5D_0$, but it pushes downward $^7F_0$ and leads to the change of the $^5D_0 \rightarrow {}^7F_0$ transition energy.

other $^7F_{J'}$ multiplet (J' = 0–6) into ^7F_J multiplets (J = 0–2) by using the Eq. (7), Table 3 and the obtained CFPs without considering J-mixing listed in Table 5. They are listed in Table 6 and only show the contributions of the CFPs with k = 2 and 4. From Table 6, it can be deduced that the mixing percentages from the $^7F_4$ state into the ground $^7F_0$ state is important for this host, and the mixing percentages from $^7F_3$ into $^7F_1$ is larger than that from $^7F_2$. The fitting calculations within ^7F_J multiplets (J = 0–2) were implemented by diagonalizing the effective Hamiltonian matrix provided by Eq. (11). In the diagonalization process, the sixth rank CFPs were neglected as an approximation although they have an influence on the higher lying stark levels of $^7F_2$. The effective Hamiltonian matrix taking all other ^7F_J mixing into account was singly diagonalized within one multiplet and $E_{cf}(^7F_J)$ (J = 0–2) can be obtained from the measurement as shown in Table 6, but the energy level fitting was carried out within the three multiplet due to simultaneously considering the second and fourth rank CFPs, whose values are also listed in Table 5, whereas Table 4 shows the calculated energy levels in comparison with the experimental data. The fitting deviation is much larger because the calculated highest Stark level of $^7F_2$ greatly deviates from the experimental one due to not considering the sixth rank CFPs. The presumed free-ion energy levels are shifted by J-mixing effect, so we calculated the positions of free-ion energy levels relation to $^7F_0$ by using Eq. (10), and collected them in Table 6. A fitting calculation of free-ion levels was also made following the same procedure in the case without J-mixing. The finally obtained F^2 and ξ_{4f} parameters were also collected in Table 5 whereas Table 6 shows the calculated free-ion energy levels.

Finally, we paid some attentions to three most pronounced Stark levels of the $^7F_1$ manifold. In the past few years, most people have adopted the approximation of only considering the second rank CFPs to analyze the J-mixing effects on the $^7F_1$ Stark levels of Eu^{3+} ions [26,27]. Although their obtained theoretical results may be used to explain their experimental ones, the values of the obtained second rank CFPs are still underestimated. In fact, the contributions of the fourth rank CFPs for the mixing from $^7F_3$ into $^7F_1$ cannot be ignored. In our case, the calculated contribution of the fourth rank CFPs is about 66% of the admixture from $^7F_3$ into $^7F_1$ by using Eq. (7), Table 3 and the obtained CFPs without considering J-mixing listed in Table 5. To show the influence of the fourth rank CFPs on the maximum CF splitting of the $^7F_1$ state, we finished two CF calculations respectively including fixed the fourth rank CFPs or not by following the method referred by Ref. [26]. The fitting calculations for $^7F_1$ was firstly carried out by only considering the second rank CFPs, and the second rank CFPs are respectively obtained as 817 cm^{-1} for B_0^2 and 327 cm^{-1} for B_2^2, which are smaller than the values in the last column of Table 5. And then we added the fixed fourth rank CFPs obtained from the last column of Table 5 to calculate the Stark levels of $^7F_1$ again. The calculated levels of $^7F_1$ and $^7F_0$ before and after adding the fourth rank CFPs are respectively listed in two columns with the name "Method C" of Table 7. From the Table 7, one can find the maximum CF splitting of $^7F_1$ is greatly compressed from 308 cm^{-1} to 216 cm^{-1} after adding the fourth rank CFPs. This means the values of the second rank CFPs must be increased to satisfy the experimental data as we expected.

As a comparison, by following the aforementioned procedure, we used Eq. (8) (i.e. our method) and the same CFPs to generate two sets of the Stark splitting of $^7F_1$ and $^7F_0$ manifolds, where $E(^7F_0)$ and $E(^7F_1)$ was set respectively equal to 0 and 383 cm^{-1} (i.e. standard values produced by free-ion calculation using the parameter values in Ref.[5]). The reason why to use Eq. (8) instead of Eq. (11) here is that the CF calculation referred by Ref. [26] is built on the free-ion calculation using the parameter values in Ref. [5]. The relative positions of the $^7F_1$ and $^7F_0$ Stark levels were collected in the Table 7, which correspond to the two columns named by "Method B" in Table 7. In addition, the methods proposed by Nishimura et al. [27] is actually the special case of our method, which means we can easily implement his calculation by limiting the summation index J' to 3 in Eq. (7) and only considering the second rank CFPs. The related calculated results are also listed in the column with the name "Method A" of Table 7. Two conclusions can also be deduced from Table 7. One is that ignoring the mixing from $^7F_{J'}$ with $J' > 3$ is reasonable for the CF splitting calculation of $^7F_1$. Another one is that the calculated results from our method coincide with those from the method referred by Ref. [26].

3.2. TiO_2:Eu^{3+}

The two phases (anatase and rutile) of titanium dioxide TiO_2 doped with trivalent rare-earth ions are widely studied due to their potential applications as phosphors [28,2], low-temperature luminescence-based gas sensing [29] and enhanced photocatalytic

Table 7
Calculated CF energy levels of $^7F_0$ and $^7F_1$ multiplets for Eu^{3+} ions doped in SnO_2 by using different approaches(unit: cm^{-1}).

Multiplets	Only considering CFPs with k = 2			Considering CFPs with k = 2 and 4	
	Method A	Method B	Method C	Method B	Method C
$^7F_0$	0	0	0	0	0
$^7F_1$	244	244	249	285	272
	398	398	396	377	373
	569	569	557	508	488

Notes: The "Method A", "Method B" and "Method C", respectively, represent the three different schemes proposed by Ref. [27], us and Ref. [26]. In all the calculations, the values of two second rank CFPs B_0^2 and B_2^2 are, respectively, fixed as 817 cm^{-1} and 327 cm^{-1}, and the other CFP values are obtained from the last column of Table 5.

Table 8
Optimized parameters for Eu^{3+} ions situated at a site of D_2 and C_{2v} symmetry in TiO_2 (unit: cm^{-1}).

Parameter	Value (C_{2v})	Value (D_2)
E_{avg}	63,614	64,718
F^2	82,256	84,685
F^4	61,248	60,381
F^6	40,411	41,288
ξ_{4f}	1,324	1,349
B^2_0	99	−24
B^2_2	−721	446
B^4_0	1079	−3733
B^4_2	−707	−1945
B^4_4	−2414	1125
B^6_0	2092	−3916
B^6_2	−1697	−1853
B^6_4	1182	171
B^6_6	1073	121
N_E (cf)	47	42
N_p (cf)	14	14
σ (cf)	31.8	33.7

Notes: The other free-ion parameters were fixed at the values given in Ref. [5]. N_E (cf) and N_p (cf) are, respectively, the numbers of crystal-field levels fitted and the numbers of freely adjustable free-ion and CFPs: $\sigma(cf) = \sqrt{\sum_{i=1,\cdots N_E(cf)}(E_i(calc.) - E_i(\exp.))^2/(N_E(cf) - N_p(cf))}$.

properties [30]. Recently [12], detailed spectroscopic study of trivalent europium in anatase TiO_2 was published. Site-selective spectroscopy methods helped in identifying three different Eu^{3+} sites denoted by them as Sites I, II, and III; detailed spectroscopic measurements resulted in obtaining positions of 26 Eu^{3+} energy levels for site I, 47 levels for site II, and 42 levels for site III. According to the assignment of Luo et al., the sites I, II and III can be respectively referred to as the sites with the site symmetry C_1, C_{2v} and D_2. For site I, there are very few (three) observed CF energy levels in ^7F_J multiplets with the larger J values ($J \geq 3$). This makes the determination of the sixth-rank CFPs difficult and the incompletely uncertain assignments of CF energy levels in these J manifolds will also lead to an unrealistic set of CFPs. In addition, much more CFPs will be further introduced for site I with lower site symmetry relative to another two sites in CF fitting calculations. Thus, we have chosen the two sets (site II and III) of Eu^{3+} experimental energy levels reported in Ref. [12] for calculations of the CFPs in the TiO_2:Eu^{3+} system. A large number of the experimental energy levels allow to vary not only 9 CFPs but also free-ion parameters, such as Slater integrals and spin-orbit coupling constant, as well.

Table 8 below shows the two sets of the free-ion's parameters and CFPs for two sites of Eu^{3+} doped in anatase TiO_2. With 47 and 42 energy levels respectively included into the fitting procedure, the rms value is respectively 31.8 cm^{-1} and 33.7 cm^{-1}, which indicates good fit quality. The next Tables 9 and 10 collect the corresponding experimental energy levels of two sites of Eu^{3+} in TiO_2 [12], in comparison with our calculated results. From Tables 9 and 10, one can find that there are large deviations between a few calculated and experimental energy levels. For instance, the largest deviation – 108 cm^{-1} – between the calculated and experimental energy levels is for one component from the $^5D_1$ level of site D_2 of Eu^{3+} (i.e. in Table 10). This shows the correlated CF effects are needed to be further considered as reported previously in the literature [31,32].

It should be emphasized that these calculations have been performed using the complete basis set of the Eu^{3+} $4f^6$ configuration, consisting of 3003 wave functions. Thus, the J-mixing effects were taken into account automatically by means of the chosen basis set. For the sake of brevity, only those energy levels which have been experimentally detected in Ref. [12] are given in Table 9. The complete calculated energy level scheme of anatase TiO_2:Eu^{3+} is available from the authors upon request.

Table 9
Observed (E_{exp}) and calculated (E_{calc}) CF energy levels of Eu^{3+} ions situated at a site of C_{2v} symmetry site in TiO_2 (unit: cm^{-1}).

Level no.	$[^{2S+1}L_J]$	E_{calc}	E_{exp}	$\Delta = E_{exp} - E_{calc}$
1.	$^7F_0$	−18	0	18
2.	$^7F_1$	226	233	7
3.	$^7F_1$	397	411	14
4.	$^7F_1$	423	435	12
5.	$^7F_2$	739	668	−71
6.	$^7F_2$	879	891	12
7.	$^7F_2$	1,092	1,060	−32
8.	$^7F_2$	1,226	1,222	−4
9.	$^7F_3$	1,801	1,819	18
10.	$^7F_3$	1,909	1,956	47
11.	$^7F_3$	1,954	1,994	40
12.	$^7F_3$	2,037	2,027	−10
13.	$^7F_3$	2,048	2,069	21
14.	$^7F_4$	2,460	2,449	−11
15.	$^7F_4$	2,658	2,618	−40
16.	$^7F_4$	2,855	2,860	5
17.	$^7F_4$	2,929	2,951	22
18.	$^7F_4$	3,061	3,072	11
19.	$^7F_4$	3,142	3,114	−28
20.	$^7F_4$	3,186	3,157	−29
21.	$^5D_0$	17,081	17,107	26
22.	$^5D_1$	18,836	18,828	−8
23.	$^5D_1$	18,877	18,861	−16
24.	$^5D_1$	18,900	18,871	−29
25.	$^5D_2$	21,278	21,247	−31
26.	$^5D_2$	21,386	21,403	17
27.	$^5D_2$	21,411	21,462	51
28.	$^5D_3$	24,109	24,093	−16
29.	$^5D_3$	24,144	24,157	13
30.	$^5D_3$	24,260	24,248	−12
31.	$^5L_6$	24,500	24,497	−3
32.	$^5L_6$	24,567	24,565	−2
33.	$^5L_6$	24,656	24,655	−1
34.	$^5L_6$	24,871	24,882	11
35.	$^5L_6$	25,107	25,143	36
36.	$^5L_6$	25,244	25,186	−58
37.	$^5L_6$	25,341	25,268	−73
38.	$^5L_6$	25,582	25,592	10
39.	$^5L_7$	25,695	25,696	1
40.	$^5L_7$	25,909	25,920	11
41.	$^5G_3$	25,979	25,991	12
42.	$^5G_3$	26,081	26,099	18
43.	$^5G_3$	26,171	26,184	13
44.	$^5G_5$	26,273	26,263	−10
45.	$^5G_5$	26,372	26,391	19
46.	$^5G_4$	26,454	26,464	10
47.	$^5G_5$	26,527	26,535	8

Notes: The standard deviation is 31.8 cm^{-1}. The symbol "$[^{2S+1}L_J]$" represents the dominative multiplet component of the crystal-field energy level.

4. Discussion of the relation between CF strength parameters and the maximum splittings of one *J* manifold (*J* = 1 and 2)

It has been shown by Auzel et al. [20] and Malta et al. [33] that the maximum crystal-field splitting of J-manifolds is a linear function of the CF strength parameters. Such a remarkable property allows for efficient and reliable estimation of the maximum splitting of particular J-manifolds (provided the set of the CFPs is known). It is also possible to evaluate the CF strength parameter from the experimental data (provided that the positions of the CF sublevels arising from a particular J-manifold are measured with good precision).

To find out how the J-mixing effects contribute to the above described relation, we considered two J-manifolds of Eu^{3+} ions ($^7F_1$ and $^7F_2$) in three hosts; SnO_2 (for which the experimental data were obtained in the present work), anatase TiO_2 (with experi-

Table 10
Observed (E_{exp}) and calculated (E_{calc}) CF energy levels of Eu^{3+} ions situated at a site of D_2 symmetry site in TiO_2 (unit: cm^{-1}).

Level no.	$[^{2S+1}L_J]$	E_{calc}	E_{exp}	$\Delta=E_{exp}-E_{calc}$
1.	$^7F_0$	−3	0	3
2.	$^7F_1$	277	278	1
3.	$^7F_1$	384	377	−7
4.	$^7F_1$	400	407	7
5.	$^7F_2$	697	677	−20
6.	$^7F_2$	875	880	5
7.	$^7F_2$	1,093	1,070	−23
8.	$^7F_3$	1,842	1,805	−37
9.	$^7F_3$	1,873	1,865	−8
10.	$^7F_3$	1,949	1,966	17
11.	$^7F_3$	1,960	1,980	20
12.	$^7F_3$	2,081	2,069	−12
13.	$^7F_3$	2,404	2,411	7
14.	$^7F_4$	2,585	2,596	11
15.	$^7F_4$	2,669	2,663	−6
16.	$^7F_4$	2,931	2,952	21
17.	$^7F_4$	3,088	3,116	28
18.	$^7F_4$	3,136	3,131	−5
19.	$^5D_0$	17,020	17,063	43
20.	$^5D_1$	18,745	18,787	42
21.	$^5D_1$	18,788	18,798	10
22.	$^5D_1$	18,914	18,806	−108
23.	$^5D_2$	21,215	21,183	−32
24.	$^5D_2$	21,317	21,341	24
25.	$^5D_3$	24,028	24,031	3
26.	$^5D_3$	24,059	24,087	28
27.	$^5D_3$	24,181	24,184	3
28.	$^5L_6$	24,400	24,406	6
29.	$^5L_6$	24,550	24,566	16
30.	$^5L_6$	24,804	24,781	−23
31.	$^5L_6$	24,907	24,904	−3
32.	$^5L_6$	25,048	25,065	17
33.	$^5L_6$	25,053	25,107	54
34.	$^5L_7$	25,182	25,190	8
35.	$^5G_3$	25,511	25,504	−7
36.	$^5L_7$	25,662	25,603	−59
37.	$^5L_7$	25,862	25,837	−25
38.	$^5G_2$	25,941	25,925	−16
39.	$^5L_7$	26,001	26,016	15
40.	$^5G_6$	26,182	26,172	−10
41.	$^5G_5$	26,282	26,299	17
42.	$^5L_7$	26,472	26,469	−3

Notes: The standard deviation is 33.7 cm^{-1}. The symbol "$[^{2S+1}L_J]$" represents the dominative multiplet component of the crystal-field energy level.

mental data for three possible sites from Ref. [12]), and ZrO_2 (with experimental data from Ref. [34], based on the energies of the following emission transitions: $^5D_0 \rightarrow {}^7F_1$ at 591.5 nm, 596.7 nm, and 598 nm). Table 11 along with Figs. 4 and 5 show the results of analysis of the $^7F_1$ and $^7F_2$ splittings without and with taking into account the *J*-mixing effects.

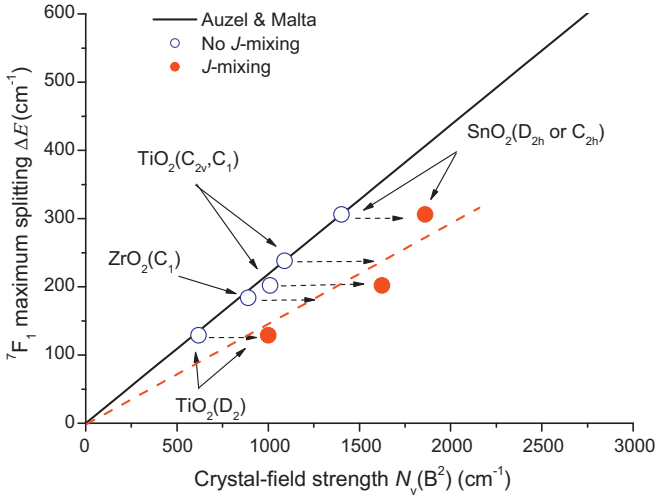

Fig. 4. Crystal-field strength parameter $N_v(B^2)$, with (filled circles) and without (open circles) taking into account the *J*-mixing vs the maximum splittings of the $^7F_1$ level for Eu^{3+} ions situated at different sites in three hosts. The dashed line is a guide to the eye; the points of its intersection with horizontal dashed arrows indicate approximate estimations of $N_v(B^2)$ for ZrO_2, TiO_2 (C_1) systems.

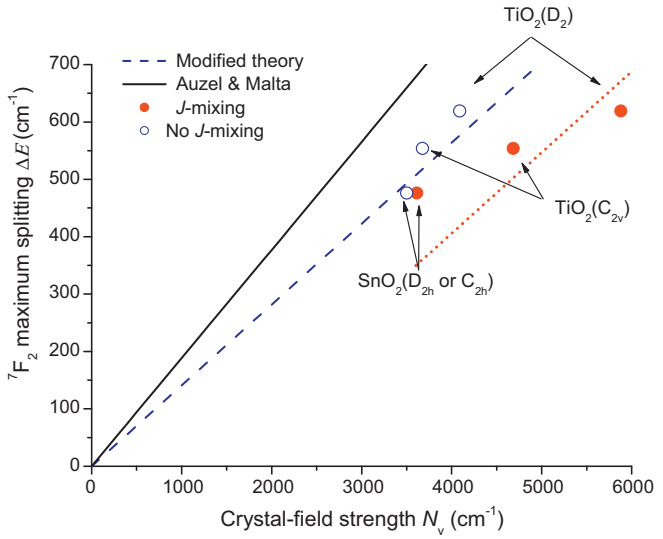

Fig. 5. CF strength parameter $N_v(=\sqrt{N_v^2(B^2)+N_v^2(B^4)})$, with (filled circle) and without (open circles) taking into account the *J*-mixing vs the maximum splittings of the $^7F_2$ level for Eu^{3+} ions doped in SnO_2 and TiO_2. The dotted line is a guide to the eye.

Table 11
The CFPs and related CF strength parameters obtained from the splitting of the $^7F_1$ and $^7F_2$ levels for Eu^{3+} ions in three different hosts (unit: cm^{-1}). The values obtained with *J*-mixing effects are given in the parentheses.

Host	Site symmetry	$^7F_1$			$^7F_2$
		B_0^2	B_2^2	$N_v(B^2)$	$N_v=\sqrt{N^2(B^2)+N^2(B^4)}$
SnO_2	D_{2h} (or C_{2h})	777 (936)	298 (501)	1401 (1861)	3499 (3612)
TiO_2	D_2	265 (−24)	202 (446)	618 (1001)	[4090] (5879)
	C_{2v}	377 (99)	363 (−721)	1010 (1624)	[3676] (4683)
	C_1	603	233	1089	–
ZrO_2	C_1	368	300	890	–

Notes: The *J*-mixing has not been considered for all the cases because there are not enough data to implement *J*-mixing calculation for every site or host. The value in the bracket was obtained from the fitting calculation of CF energy levels within the separate multiplet $^7F_2$ where the theoretical CF energy levels were including in the fitting calculation due to the lack of experimental data.

4.1. $J = 1$

If only a single $^7F_1$ level is considered, then determination of the B_0^2, B_2^2 parameters is straightforward. In the $J = 1$ case the obtained $N_v(B^2)$ values excellently follow the straight line predicted by Malta et al. in their Ref. [33] (Fig. 4). The proportionality constant between the maximum splitting and the CF strength parameter is about 0.218 if the α parameter in Eq. (7) of Ref. [33] is regarded as 0 in a good approximation due to the symmetrical splitting observed for the $^7F_1$ level. However, if the $^7F_2$ and $^7F_3$ perturbation terms are added (SnO_2 and TiO_2 (D_2 and C_{2v}) systems), the CFPs should be increased, in order to fit the experimental splittings of both states. Such a behavior of CF strength is illustrated by the horizontal dashed arrows in Fig. 4; it can be explained by repulsion of the CF energy levels between $J = 1$ and $J = 2$ and 3 manifolds, which can be compensated by corresponding increase of CFPs. This observation leads to the conclusion that if the CFPs obtained from fitting of the $J = 1$ states only are used to calculate the CF splitting in a larger basis set, reliable reproduction of the experimental results would not be possible. As a consequence, re-fitting procedure (which results in an increase of the CFPs) should be used if such an enlarged basis set is employed in the CF calculations.

The dashed line in Fig. 4 goes through three data points of the J-mixing calculations as a guide to the eye. Since not enough experimental levels were given for ZrO_2, TiO_2 (C_1) systems, the J-mixing calculations are not possible. Nevertheless, approximate estimations of the CF strength parameter $N_v(B^2)$ for ZrO_2 (as 1345 cm^{-1}) and TiO_2(C_1) (as 1632 cm^{-1}) can be easily obtained from Fig. 4.

4.2. $J = 2$

Maximum splitting of the $^7F_2$ level is depicted in Fig. 5. The straight line here is the maximum splitting of the $^7F_2$ as described by Auzel et al. [20], and the dashed line is a plot of the following equation:

$$\Delta E = \left[\frac{3g_a^2}{g(g_a+2)(g_a+1)\pi}\right]^{1/2} \times \left[\prod_{k=2,4} \left|\left\langle 4f^6[\eta SL]2 \left\| U^{(k)} \right\| 4f^6[\eta SL]2 \right\rangle \left\langle f \left\| c^{(k)} \right\| f \right\rangle\right|\right]^{1/2} N_v, \quad (12)$$

where $N_v = \sqrt{N_v^2(B^2) + N_v^2(B^4)}$ is the CF strength parameter for the $J = 2$ manifold, g is the state number of this manifold (i.e. 5), and g_a equal to g is the degeneracy effectively removed by field. $\langle 4f^6[(SL]2||U^{(k)}||\ 4f^6[(SL]2\rangle$ and $\langle f||c^{(k)}||f\rangle$ are the *RME* of the multi-electron unit tensor $U^{(k)}$ and the single-electron spherical harmonic tensor $c^{(k)}$, respectively.

This equation has been derived similarly to Eq. (15) of Ref. [20], with that difference that only CFPs of the second and fourth rank are considered (since the matrix elements of the CF Hamiltonian are zero on the wave function of the $J = 2$ manifolds, if the sixth rank operators are considered). The only difference between Eq. (12) we proposed and Eq. (15) of Ref. [20] happens upon the power of the absolute value of the product of all the RMEs of the multi-electron tensor $C^{(k)}$ (defined by Wybourne [6]) within one J manifold. This originates from the approximation proposed by Auzel et al. (i.e. Eq. (14) of Ref. [20]) is not held in general. This approximation actually presents the viewpoint that one quadratic equation of a quadric surface in the k-space (k is CFPs rank) can be replaced by a sphere of the same volume, which implies the dimension of k-space must be three. For those manifolds with larger J value ($J \geq 3$), it is very suitable and right as shown in a lot of successful applications of their theory of Ref. [20], because the possible values of k are equal to 2, 4 and 6 according to the selection rule ($k \leq 2J$) (i.e. three dimensional k-space). But for these manifolds with $J = 1$ or 2, the possible values of k are respectively equal to 2, or 2 and 4, which means the three dimensional k-space (3-D) essentially degenerate into 2-D or 1-D. Thus, their viewpoint shall be further modified as that one quadratic equation of a quadric surface or curve in the k-space can be replaced by a sphere or circle of the same volume or area, and the power must be written as 1/3 for 3-D and 1/2 for 2-D. For 1-D case, this approximation can be skipped as shown in Ref. [33] (i.e. the power is 1).

As seen from Fig. 5, the estimations of the $^7F_2$ maximum splitting for SnO_2 and TiO_2 (D_2 and C_{2v}) closely follow the solid line of Eq. (12). The proportionality constant between the maximum splitting and the CF strength parameter is about 0.141. In addition, similarly to the previous case of the $^7F_1$ manifold, inclusion of the J-mixing effects implies increase of the CFPs values, if the experimental splitting is to be kept as close as possible to the calculated results. Absolute value of the CF strength parameter increases significantly with increase of the maximum splitting; it varies only from 3499 cm^{-1} to 3612 cm^{-1} for SnO_2 (with the $^7F_2$ splitting 476 cm^{-1}) and it changes more significantly from 4090 cm^{-1} to 5879 cm^{-1} for D_2 site of TiO_2 (when the $^7F_2$ splitting equals to 621 cm^{-1}) and from 3676 cm^{-1} to 4683 cm^{-1} for C_{2v} site of TiO_2 (when the $^7F_2$ splitting equals to 554 cm^{-1}). According to the analysis of J-mixing for $^7F_1$ state, three data points of the J-mixing calculations for $^7F_2$ state can be expected to be uniformly distributed nearby the dotted line as plotted in Fig. 5. But the data point of SnO_2 deviates from the assumption. This is because the theoretical energy position of the highest-lying CF energy level of $^7F_2$ state is overestimated due to ignoring the sixth rank CFPs in the J-mixing calculation for SnO_2, which leads to the underestimate of the CF strength parameter. Thus, to obtain the accurate CFPs, the experimental CF energy level of $^7F_3$ or high-lying ^7F_J maybe need to be known as discussed in Section 2.

These examples unambiguously show importance of proper consideration of J-mixing effects for analysis of CF splitting of Eu^{3+} energy levels, thus urging to use as large basis set as possible. Even when excellent fittings can be performed for the $^7F_1$ and $^7F_2$ manifolds with very small rms deviation between the calculated and experimental energy levels, the obtained sets of CFPs are by no means fully applicable to calculations of CF splitting of other manifolds, but rather provide a lower estimate of the actual CFPs, which would lead to considerable underestimation of the experimentally measured CF splitting of the high-lying manifolds.

5. Conclusion

In the present work we have calculated the energy level schemes of Eu^{3+} ions in a number of metal oxide matrices. A perturbation-theory based approach developed in the present paper, allowed to quantify the J-mixing effects (produced by CF interactions) by evaluating the actual composition of the J-states in terms of the CF strength parameters. Inclusion of non-negligible contribution from higher located J-manifolds is crucial for modeling the CF splittings and intensities of the electric-dipole transitions. In addition, the relation between the maximum CF splittings and CF strength parameter for $^7F_2$ state was discussed for the first time, and the original theory proposed by Auzel et al. was further developed. The modified theory can also be applied to the manifold with $J = 1/2$ and 5/2 (here the value of J should satisfy the condition $0 < J < 3$, due to the above-mentioned CF operators selection rules).

The developed method of analysis of the Eu^{3+} energy level scheme has been successfully tested on three Eu^{3+}-doped hosts: (i) SnO_2 (cassiterite); (ii) TiO_2 (anatase); (iii) ZrO_2 (monoclinic). Good agreement between the calculated and experimentally derived

energy level schemes serves as an indication of correctness of the suggested model. As a result of the performed CF analysis, reliable sets of CFPs have been obtained for all systems.

The *J*-mixing effects were proven to be of crucial importance for getting reasonable agreement between the calculated and experimental energy levels. In the simulation of the CF splittings of ^7F_J state ($J = 1$ or 2) when considering *J*-mixing effect, our calculation showed that the neglect of the CFPs with rank $k = 2J + 2$ will lead to significant underestimation of all CFPs values. Separate consideration of the CF splitting of individual manifolds – although quite often used in the literature – cannot produce a suitable set of CFPs, but, in the best case, gives the lowest CFPs estimate.

A similar consideration of treating the *J*-mixing effects can be performed for other rare-earth ions.

Acknowledgement

Financial support from Estonian Science Foundation grants nos. 7456, 6999, 6658 and 7612GLOFY054MJD is gratefully acknowledged. The authors thank Prof. P.A. Tanner (City University, Hong Kong) for valuable and fruitful discussions.

References

[1] S. Lange, I. Sildos, V. Kiisk, J. Aarik, M. Kirm, Phys. Status Solidi (c) 2 (2005) 326.
[2] V. Kiisk, V. Reedo, O. Sild, I. Sildos, Opt. Mater. 31 (2009) 1376.
[3] V. Kiisk, T. Kangur, T. Tätte, I. Sildos, Terrae Rarae, in: G. Meyer (Ed.), Proceedings of ICFE-7, Cologne, Germany, 2009.
[4] G.K. Liu, in: G.K. Liu, B. Jacquier (Eds.), Spectroscopic Properties of Rare Earths in Optical Materials, Tsinghua University Press & Springer-Verlag (Berlin), Heidelberg, 2005, p. 1.
[5] W.T. Carnall, G.L. Goodman, K. Rajnak, R.S. Rana, J. Chem. Phys. 90 (1989) 3443.
[6] B.G. Wybourne, Spectroscopic Properties of Rare Earths, Interscience Publishers (John Wiley & Sons, Inc.), New York, 1965.
[7] P. Caro, O. Beaury, E. Antic, J. Phys. (France) 37 (1976) 671.
[8] G.J. McCarthy, J.M. Welton, Powder Diffr. 4 (1989) 156.
[9] D.F. Crabtree, J. Phys. D: Appl. Phys. 8 (1975) 107.
[10] V. Kiisk, V. Reedo, M. Karbowiak, M.G. Brik, I. Sildos, J. Phys. D: Appl. Phys. 42 (2009) 12517.
[11] E.F. Lopez, V.S. Escribano, M. Panizza, M.M. Carnasciali, G. Busca, J. Mater. Chem. 11 (2001) 1891.
[12] W.Q. Luo, R.F. Li, G.K. Liu, M.R. Antonio, X.Y. Chen, J. Phys. Chem. (c) 112 (2008) 10370.
[13] C. Görller-Walrand, K. Binnemans, in: K.A. Gschneidner Jr., L. Eyring (Eds.), Handbook on the Physics and Chemistry of Rare Earths, vol. 23, North-Holland Publishing Company (Elsevier), Amsterdam, 1996, pp. 121.
[14] P.A. Tanner, Top. Curr. Chem. 241 (2004) 167.
[15] M. Rotenberg, R. Biyins, N. Metropolis, J.K. Wooten, The 3-j and 6-j Symbols, M. I. T. Press, Cambridge, MA, USA, 1959.
[16] C.A. Morrison, R.P. Leavitt, in: K.A. Gschneidner Jr., L. Eyring (Eds.), Handbook on the Physics and Chemistry of Rare Earths, vol. 5, North-Holland Publishing Company (Elsevier), Amsterdam, 1982, pp. 461.
[17] C. Rudowicz, R. Bramley, J. Chem. Phys. 83 (1985) 5192.
[18] C.W. Nielson, J.F. Koster, Spectroscopic Coefficients for the p^n, d^n and f^n Configuration, M. I. T. Press, Cambridge, MA, USA, 1963.
[19] W.T. Carnall, H. Crosswhite, H.M. Crosswhite, Energy level structure and transition probabilities in the spectra of the trivalent lanthanides in LaF_3, Argonne National Laboratory, Argonne, IL, USA, 1978.
[20] F. Auzel, O.L. Malta, J. Phys. (France) 44 (1983) 201.
[21] H.L. Wen, G.H. Jia, C.K. Duan, P.A. Tanner, Phys. Chem. Chem. Phys. 12 (2010) 9933.
[22] V. Hurtubise, K.F. Freed, J. Chem. Phys. 100 (1994) 4955.
[23] V. Kiisk, T. Kangur, M. Paalo, T. Tätte, S. Pikker, I. Sildos, Phys. Status Solidi (c), Conference paper (ICOOPMA10: A-0156), in press (2011).
[24] T.T. Zhang, K.W. Li, J. Zeng, Y.L. Wang, X.M. Song, H. Wang, J. Phys. Chem. Solids 69 (2008) 2845.
[25] G. Blasse, J. van Keulen, Chem. Phys. Lett. 124 (1986) 534.
[26] V. Lavin, P. Babu, C.K. Jayasankar, I.R. Martin, V.D. Rodriguez, J. Chem. Phys. 115 (2001) 10935.
[27] G. Nishimura, T. Kushida, Phys. Rev. B 37 (1988) 9075.
[28] S. Lange, I. Sildos, V. Kiisk, J. Aarik, Mater. Sci. Eng. B 112 (2004) 87.
[29] V. Reedo, S. Lange, V. Kiisk, A. Lukner, T. Tätte, I. Sildos, Proc. SPIE 5946 (2005) 59460F.
[30] M. Bettinelli, A. Speghini, D. Falcomer, M. Daldosso, V. Dallacasa, L. Roman, J. Phys.: Condens. Matter 18 (2006) S2149.
[31] B.R. Judd, Phys. Rev. Lett. 39 (1977) 242.
[32] O.K. Moune, P. Caro, J. Less-Common Met. 148 (1989) 181.
[33] O.L. Malta, E. Antic-Fidancev, M. Lemaitre-Blaise, A. Milicic-Tang, M. Taibi, J. Alloys Compd. 228 (1995) 41.
[34] A. Speghini, M. Bettinelli, J. Mater. Res. 20 (2005) 2780.